# Mitigating stochastics in EUV lithography by directed self-assembly

L. Verstraete*[a], Hyo Seon Suh[a], Julie Van Bel[a], Purnota Hannan Timi[a], Remi Vallat[a], Philippe Bezard[a], Jelle Vandereyken[a], Matteo Beggiato[a], Amir-Hossein Tamaddon[a], Christophe Beral[a], Waikin Li[a], Mihir Gupta[a], Roberto Fallica[a]

[a]imec, Kapeldreef 75, 3001 Leuven, Belgium

*Corresponding email: Lander.Verstraete@imec.be

## ABSTRACT

Owing to photon shot noise and inhomogeneous distribution of the molecular components in a chemically amplified resist, resist patterns defined by extreme ultraviolet (EUV) lithography tend to suffer from stochastic variations. These stochastic variations are becoming more severe as critical dimensions continue to scale down, and can thus be expected to be a major challenge for the future use of single exposure EUV lithography. Complementing EUV lithography with directed self-assembly (DSA) of block-copolymers provides an interesting opportunity to mitigate the variability related to EUV stochastics. In this work, the DSA rectification process at imec is described for both line/space (L/S) and hexagonal contact hole (HEXCH) patterns. The benefits that rectification can bring, as well as the challenges for further improvement are being addressed based on the current status of imec's rectification process.

**Keywords:** directed self-assembly, EUV lithography, pattern rectification, PS-*b*-PMMA, line/space pattern, hexagonal contact hole pattern

## 1. INTRODUCTION

Single exposure extreme ultraviolet (EUV) lithography can alleviate the complexity of ArFi-based multipatterning techniques and will allow further scaling of device features. Compared to ArFi lithography operating at a wavelength of 193 nm, EUV photons have a wavelength of 13.5 nm. For a given dose and absorbance of the photoresist, the number of photons available to define the pattern are thereby drastically reduced in case of EUV lithography.[1] As a consequence, photon shot noise might induce stochastic variations in the printed resist patterns (*i.e.* dimensional non-uniformity and associated defects). This stochastic variability is furthermore enhanced by the fact that the molecular components in a chemically amplified resist are not homogeneously distributed at the dimensions being targeted for single EUV exposures.[2] As critical dimensions of the desired patterns continue to shrink, controlling EUV stochastics will only become more important.[3]

Directed self-assembly (DSA) provides an alternative patterning solution amenable to semiconductor applications.[4,5] DSA uses a lithographically defined guide pattern to leverage the phase separation of block copolymers (BCP) to create well-defined structures. When using lamellae forming block copolymers, nanoscale line/space (L/S) structures can be formed under the right boundary conditions for self-assembly. Similarly, hexagonal contact hole (HEXCH) patterns can be created when using a cylinder forming BCP material. As the properties of these BCP structures are defined by the self-assembly process, the stochastic variability of EUV resist patterns can be avoided. In this regard, DSA has been suggested as a solution to rectify EUV resist patterns.[6,7] EUV and DSA patterning are thus complementary technologies.

In this work, imec's DSA rectification process for EUV L/S and HEXCH patterns is described. For L/S patterns, roughness is an important parameter to control.[8] However, optimization of the roughness for DSA rectified patterns will not be addressed here, but is described in an accompanying paper.[9] Instead, the focus will be on characterizing defectivity of the rectified L/S patterns. While, DSA can rectify defects in the EUV resist pattern, the DSA process itself needs to be optimized to achieve best defectivity of the rectified patterns. Moving to HEXCH patterns then, metrics of interest include the local critical dimension uniformity (LCDU), ellipticity, and pattern placement error (PPE). A comparison of these metrics for the original EUV resist pattern, as well as for the DSA rectified pattern is provided.

Novel Patterning Technologies 2023, edited by J. Alexander Liddle, Ricardo Ruiz,
Proc. of SPIE Vol. 12497, 124970I · © 2023 SPIE
0277-786X · doi: 10.1117/12.2657939

Furthermore, efforts for improving these metrics by optimizing the DSA process conditions are discussed. Finally, the possibility to print EUV HEXCH patterns with lower dose followed by DSA rectification is investigated.

## 2. METHODOLOGY

### 2.1 Rectification process

The process flow used in this work for rectification of L/S and HEXCH patterns is schematically shown in Figure 1 and Figure 2, respectively. A thin cross-linked polystyrene (X-PS) underlayer is coated first on a 300 mm Si wafer, followed by a single patterning EUV exposure step on ASML's NXE:3400B scanner. Following previous description in the literature, an oxidizing plasma is used the modify the surface energy of the X-PS areas in the trenches/holes of the photoresist pattern.[10] After stripping the remaining photoresist with Microstrip®6800, a poly(styrene-*block*-methyl methacrylate) (PS-*b*-PMMA) block copolymer (BCP) is spincoated on the guide pattern and annealed under a low oxygen environment on a DT-3000 track from SCREEN. In case of L/S patterns, a lamellae forming BCP is used and the BCP patterns are transferred into a 13 nm SiN hard mask layer by dry etch. For HEXCH patterns, a cylinder forming BCP material is coated. The PMMA cylinders are first removed by a wet development process on the DT-3000 track. Afterwards the hole pattern is transferred into a 13 nm SiN hard mask.

The rectification process is illustrated for a pitch 28 nm L/S EUV resist pattern in Figure 1. On purpose, the EUV exposure conditions were chosen to be sub-optimal resulting in a high number of defects in the EUV resist pattern. After the DSA rectification process is completed and the pattern is etched into the 13 nm SiN hard mask, no more defects are visible. Similarly, in Figure 2, the rectification process is illustrated for a $pitch_{C2C}$ 36 nm HEXCH pattern. Again, the EUV exposure conditions were deliberately sub-optimal to visualize the defect healing capability by DSA rectification.

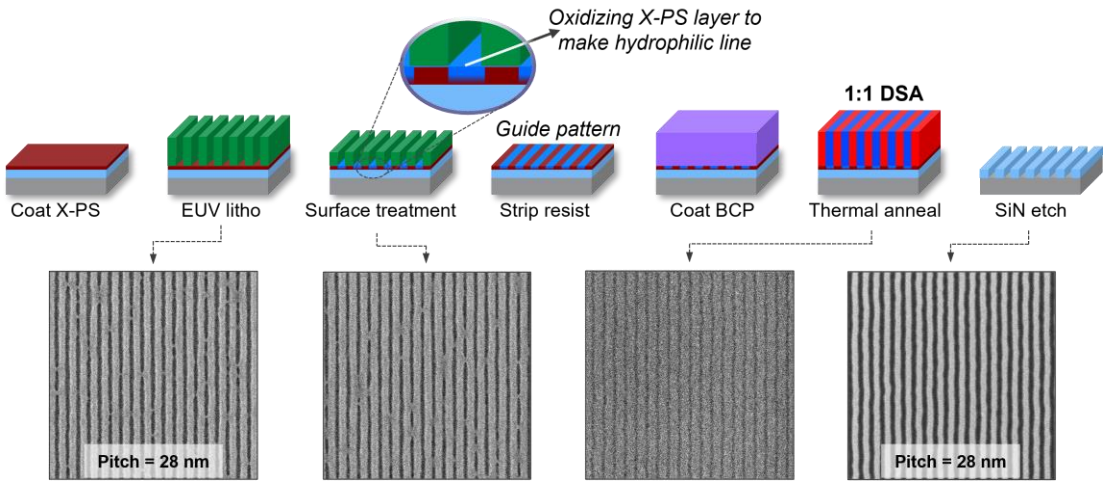


Figure 1. Schematic illustration of the DSA rectification process for EUV L/S patterns. Crucial in this process is the surface treatment that alters the surface energy of the X-PS selectively in the trenches of the photoresist pattern. Below the schematic of the process, a series of CDSEM images are shown to illustrate the rectification ability of DSA for a pitch 28 nm EUV resist pattern. The EUV resist pattern was printed with sub-optimal exposure conditions to increase the defect density (bridge defects) of the starting pattern. After the DSA process and pattern transfer into 13 nm SiN hard mask, the defects from the EUV resist pattern are healed.

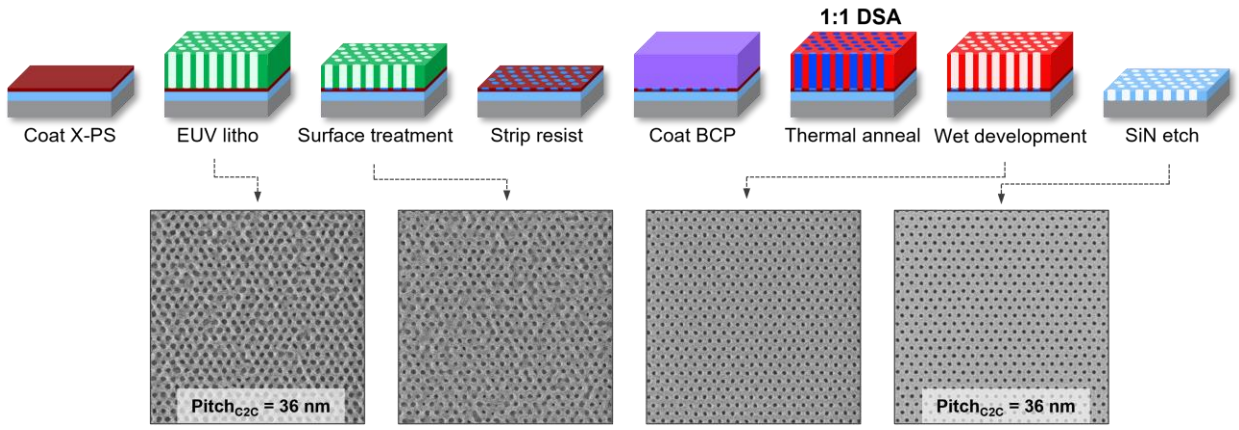


Figure 2. Schematic illustration of the DSA rectification process for EUV HEXCH patterns. The process conditions are the same as used for rectification of L/S patterns, except that a cylinder forming BCP material is coated and that the PMMA cylinders are removed by a wet development process prior to dry etch for pattern transfer to 13 nm SiN. Below the process schematic, a series of CDSEM image illustrate the rectification ability for a highly defective pitch$_{C2C}$ 36 nm HEXCH EUV pattern (printed with sub-optimal exposure conditions for illustrative purpose).

### 2.2 Characterization

Patterns on the wafer were examined using a Hitachi CG-6300 critical dimension scanning electron microscopy (CDSEM) tool. For analysis of bridge defects from CDSEM images, imaging conditions were chosen as follows: *magnification* = 82.400; *pixels* = 2048×2048; *number of frames* = 32; *number of images* = 30. For measurement of LCDU, PPE and ellipticity, the following imaging conditions were used: *magnification* = 82.400; *pixels* = 2048×2048; *number of frames* = 16 (after wet development) or 32 (after SiN etch); *number of images* = 20; *scan type* = Mobius (non-unique). All metrology was performed by offline image analysis using MetroLER™ version 3.1.5.0 (Fractilia, LCC). Shown error bars represent the standard error of the mean (as measured from one wafer). In case of PPE, the average of X PPE and Y PPE is taken and reported.

Optical defect inspection of pitch 28 nm L/S patterns etched into 13 nm SiN was performed on a KLA-Tencor 2935 inspection tool operating in dark field mode. Subsequent defect review was performed using a KLA-Tencor ebeam review (EDR7380) tool, and defects were classified manually. Defectivity analysis of HEXCH patterns after etch into 13 nm SiN was performed by acquiring a large number of SEM images on an Provision2E tool from Applied Materials. Imaging conditions used to acquire the images are: *field of view* = 2 µm×2 µm; *pixels* = 1000×1000; *number of frames* = 16. Analysis of defects for HEXCH patterns was performed by using the image processing sequence shown in Figure 3 (performed offline with the ImageJ open software package) for defect detection, followed by manual classification.

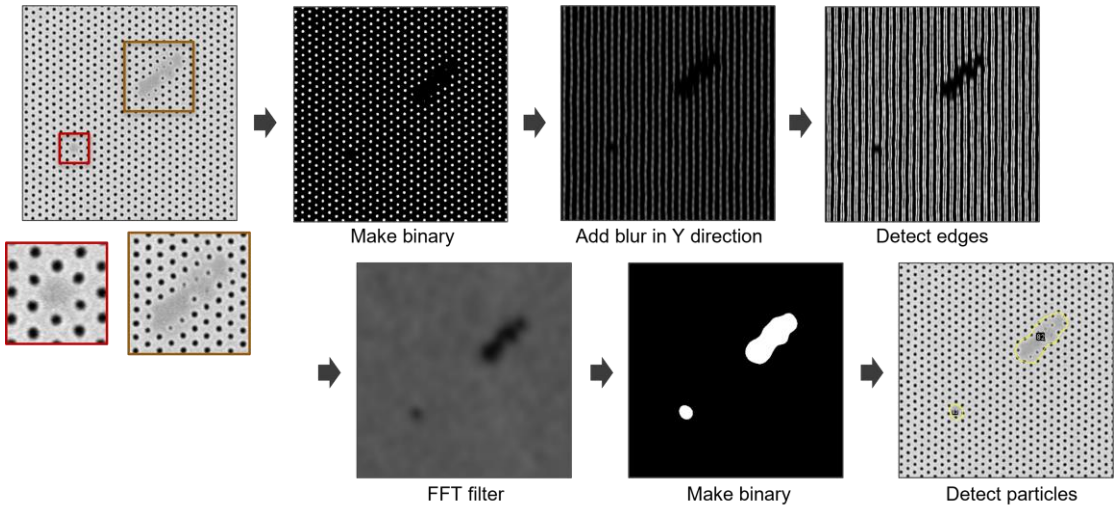


Figure 3. Image processing sequence applied for detection of defects from SEM images of HEXCH patterns obtained after etch into a 13 nm SiN hard mask. Image processing is performed offline using the ImageJ open software package. Both small defects such as a missing holes (red) and larger defects such as closed patches (brown) can be detected accurately and simultaneously.

## 3. RESULTS AND DISCUSSION

### 3.1 Pitch 28 nm L/S patterning

While the rectification ability of DSA is qualitatively shown in Figure 1 for a pitch 28 nm L/S pattern, a quantitative defect assessment of the rectified patterns on a wafer scale is desired to understand the different types of defects occurring and their density. To this end, an EUV pattern with fixed CD was printed across the whole wafer and the DSA rectification process was applied as described above. The BCP film was thermally annealed at 290 °C for 30 minutes. After pattern transfer of the DSA pattern to 13 nm SiN, optical defect inspection was used to detect potential defects. In total, 3168 defects were detected across a total inspection area of 17.5 $cm^2$, and all defects were reviewed and classified. 61% of the detected defects could be excluded as being SEM non-visible meaning that they were falsely identified as defects by the optical inspection tool. After excluding the SEM non-visible defects, a defect distribution as shown in Figure 4a was found. A first encouraging observation is that only one dislocation and one line break defect were found. The fact that only one dislocation defect was formed evidences that the kinetics of this 1-to-1 DSA process are not a roadblock and annealing times may be significantly shortened from the 30 minutes used here. Optimization of the annealing conditions is investigated and described in an accompanying paper.[9] Furthermore, the main defect type are bubble defects. As shown in Figure 4b, these bubble defects tend to appear more towards the edge of the wafer. The origin of these bubble defects is currently under further investigation. Finally, it can be observed that different types of bridge defects (single and multiple period bridges, baby bridges) are present across the whole wafer with a total density around 40 defects/$cm^2$. Reduction of bridge defects through material and process optimization is the topic of ongoing research.

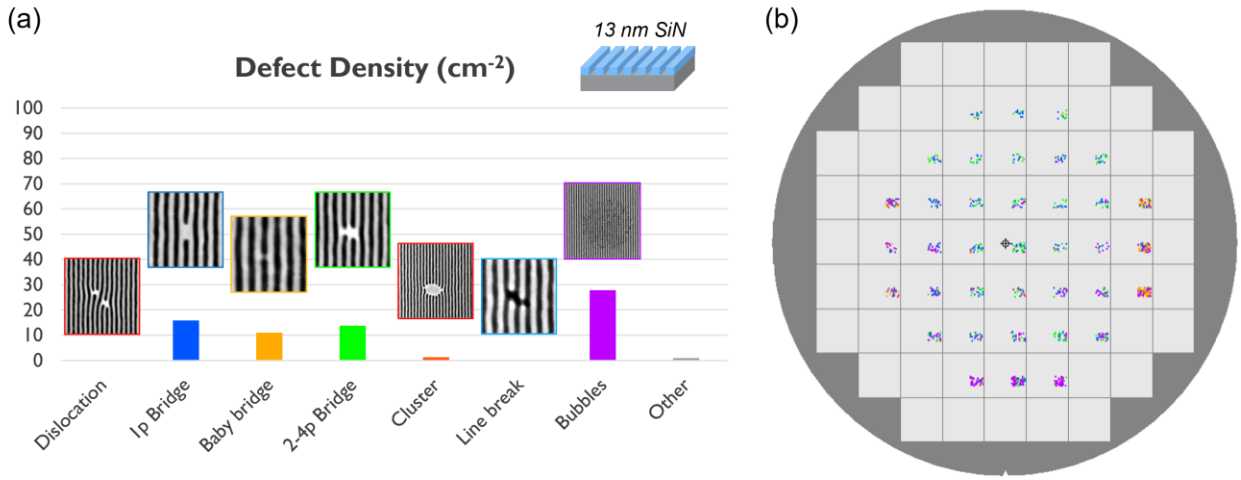


Figure 4. (a) Defect density distribution of a pitch 28 nm L/S pattern after DSA rectification. Defectivity was measured by optical inspection after etching the DSA pattern into a 13 nm SiN hard mask. For each defect type, a representative SEM image is shown. (b) Corresponding wafer map showing the defect distribution across the wafer. Color code corresponds to the colors used in (a).

### 3.2 Pitch 24 nm L/S patterning

To assess the current performance of the DSA rectification process at pitch 24 nm, CDSEM images after pattern transfer of the BCP film to 13 nm SiN were acquired as shown in Figure 5a. As can be seen from the CDSEM image, there is a high propensity for bridge type defects to be formed. A possible root cause for such bridge defects to be formed are excess polystyrene residues inside the block copolymer film. To verify whether this is the case in the BCP film under investigation here, a non-selective dry etch process was used to selectively thin down the BCP film.[11] At every interval, CDSEM images were taken to check the presence of possible residues inside the BCP film. As shown in Figure 5b, such residues were indeed observed after removing the top 66% and more of the BCP film. This experiment thus strengthens the believe that the high propensity for bridge defects after pattern transfer are caused by excess polystyrene residues in the BCP film. To reduce the number of bridge defects of the DSA rectified patterns, the BCP formulation was adjusted as shown in Figure 6. By moving from BCP A to BCP C, the number of bridge defects could be reduced by a factor of three. This result indicates that adjusting the BCP formulation is a powerful knob to control the number of bridge defects and gives room for further improvements.

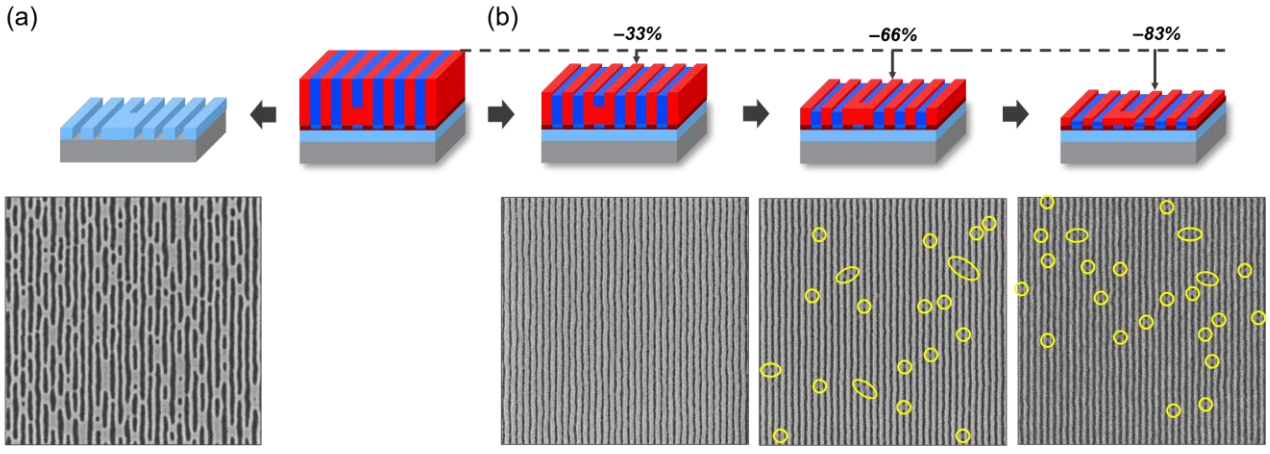


Figure 5. (a) Pattern transfer of a pitch 24 nm L/S pattern after DSA rectification to a 13 nm SiN hard mask. From a single CDSEM image, a high number of bridge defects can be observed. (b) Non-selective dry etch to thin down the BCP film in discrete steps. After removing 66% or more of the total film thickness, residues inside the BCP film can clearly be observed by CDSEM (highlighted by the yellow circles).

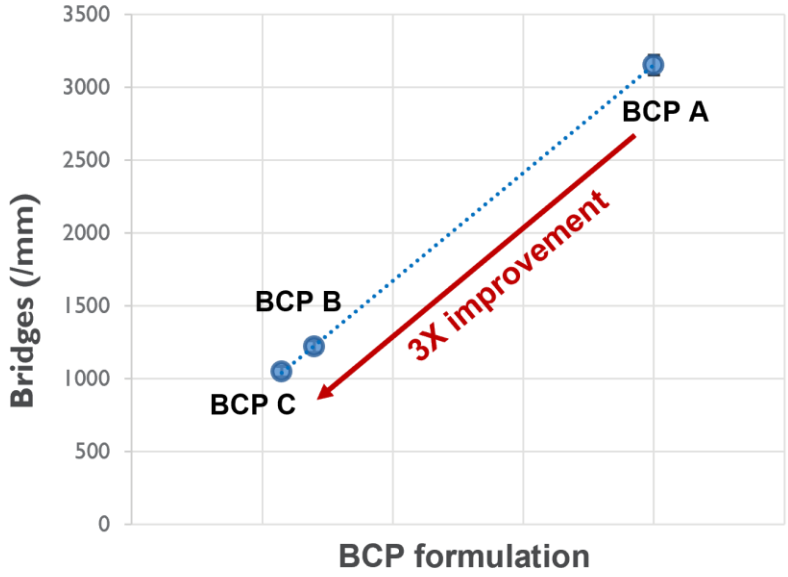


Figure 6. Impact of BCP formulation on the number of bridge defects detected after pattern transfer of the BCP film to 13 nm SiN (*pattern pitch* = 24 nm). Bridge defect number is evaluated from analysis of 30 CDSEM images as described in the methodology section. By adjusting the BCP formulation, the bridge defect density can be improved by a factor of three.

### 3.3 Pitch$_{C2C}$ 36 nm HEXCH patterning

To assess the performance of the rectification process for pitch$_{C2C}$ 36 nm HEXCH patterns, the LCDU, ellipticity and PPE were characterized throughout the process as shown in Figure 7. In terms of the LCDU, the pattern quality is improved from 2.26 nm to 1.52 nm after the DSA rectification process and pattern transfer. Whereas the LCDU of the resist pattern depends on the material-photon interaction during exposure, LCDU of the DSA rectified pattern is determined by the BCP material properties. As such, random pattern variations due to EUV stochastics can be avoided, and the LCDU is improved. Next, the ellipticity of the holes was evaluated. In this terminology, lower ellipticity refers to more circular holes and is thus desired. Looking at the data, the ellipticity of the DSA pattern after wet development of the PMMA domain is significantly higher than that of the EUV resist pattern. However, after pattern transfer to 13 nm SiN the ellipticity is being restored. The reason that ellipticity drops during the pattern transfer process can be understood by taking into account that the ellipticity obtained after wet development only characterizes the top interface of the BCP film. It is likely that the ellipticity is not constant throughout the vertical direction of the BCP film, such that during pattern transfer an overall average shape of the cylinders is etched into the SiN layer. Finally, the PPE was evaluated. PPE refers to the placement error of the cylinder with respect to its target position. As shown in Figure 7, the PPE is substantially increasing by the DSA rectification process, also after pattern transfer to SiN. Therefore, finding strategies to control the PPE of the DSA patterns is identified as a crucial requirement for further process improvement.

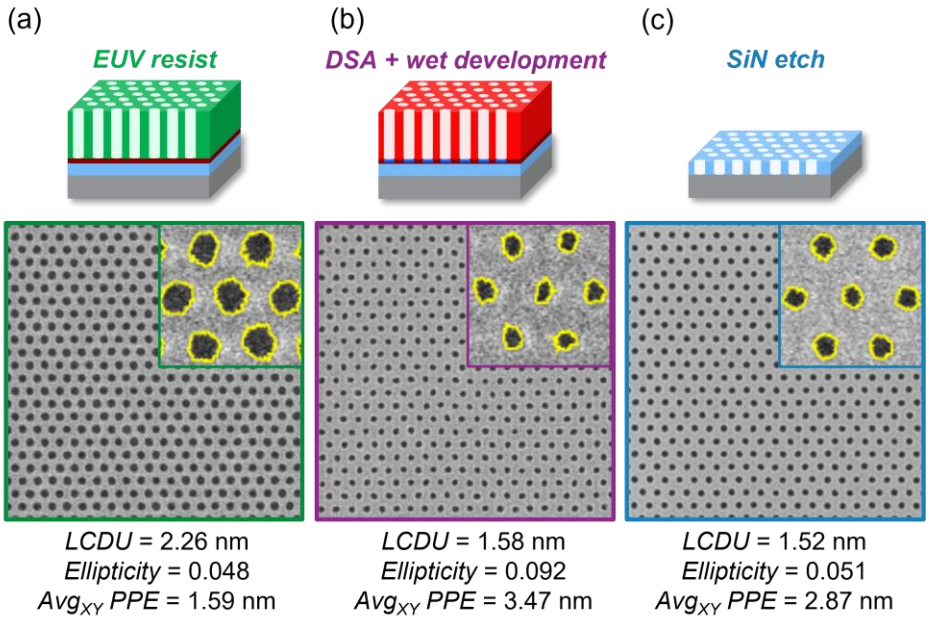


Figure 7. LCDU, ellipticity, and PPE measurement for (a) EUV resist pattern, (b) DSA rectified pattern after PMMA removal by wet development, and (c) DSA rectified pattern after pattern transfer to 13 nm SiN. Pitch of the pattern is 36 nm contact-to-contact.

Several process knobs were investigated with the goal of improving the PPE of the DSA pattern. First, the impact of BCP film thickness was studied. As shown in Figure 8, by increasing the BCP film thickness from 36 nm to 54 nm, the LCDU is slightly increasing. For the PPE value, an increase is observed after wet development, but a significant reduction is observed after etch into 13 nm SiN. This discrepancy can again be attributed to the fact that only the top interface is being considered after wet development, and thus information about the complete BCP structure is missing. Therefore, the PPE value after SiN etch is considered more relevant. Looking at the ellipticity, smaller values are obtained for thicker BCP films. Overall, it is concluded that increasing the BCP film thickness is beneficial for the overall pattern quality, mainly owing to the large PPE reduction after SiN etch.

Secondly, the dry etch time to break through the X-PS underlayer after PMMA removal by wet development is investigated. This dry etch step is necessary as the X-PS layer needs to be opened first before the BCP structure can be transferred into the SiN hard mask layer. As shown in Figure 8, increasing the dry etch time for breaking through the X-PS layer by 30% and 60% is beneficial for all three metrics considered in this study. Further increase of the dry etch time is currently under investigation.

Finally, the possibility to add a second thermal anneal step at lower temperature following the initial thermal anneal at higher temperature is studied. Specifically, a first bake is performed at 250 °C for 30 minutes, and a second bake at 200 °C, 180 °C and 160 °C for 2 hours is added. In between the two bakes, the sample is cooled rapidly to room temperature. During the first bake at high temperature, it is believed that the PMMA cylinders are fluctuating considerably on top of the guide pattern due to its thermal energy. During a rapid cool down to room temperature, the fluctuations might by locked in leading to high PPE values. Therefore, it was reasoned that adding a second bake at lower temperature might be an effective strategy for releasing the locked in PPE. However, as shown in Figure 8, the impact of such second anneal on the PPE is very limited. Nonetheless, addition of a second bake does seem to further improve the LCDU of the DSA pattern.

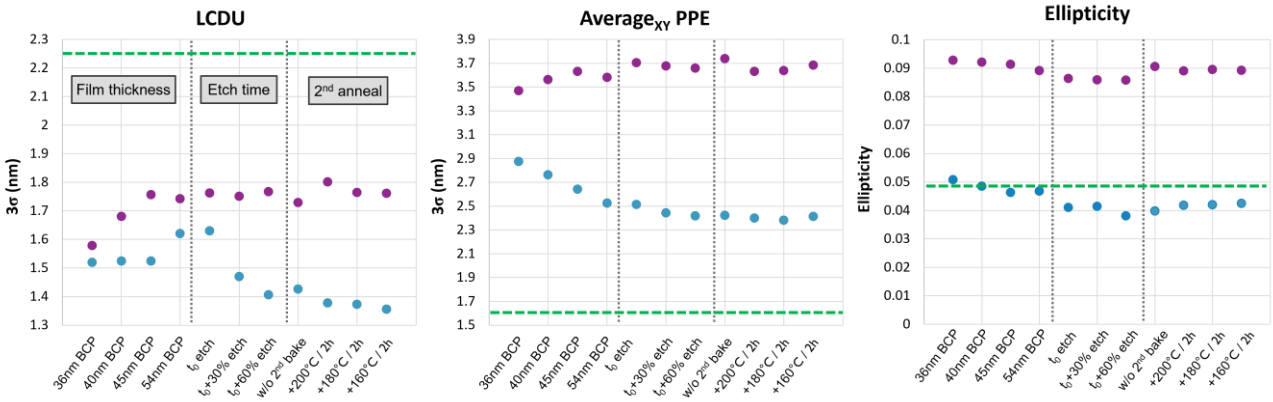


Figure 8. Characterization of LCDU, PPE, and ellipticity as a function of BCP film thickness, dry etch time to break through the X-PS underlayer after PMMA removal by wet development, and addition of a second annealing step at lower temperature following an initial thermal anneal at 250 °C for 30 minutes. Green dashed line represents the value measured from the EUV resist pattern for reference; purple data points are obtained after DSA + wet development; blue data points are obtained after pattern transfer of the DSA pattern into 13 nm SiN. Pitch of the pattern is 36 nm contact-to-contact.

Besides the metrics described above, the defectivity after DSA rectification should also be considered. To this end, defectivity was analyzed for two different DSA processing conditions and for different sizes of the guide pattern, as shown in Figure 9. The size of the guide pattern refers to the CD of the hole as measured from the EUV resist pattern and was tuned by changing the EUV exposure dose. For the defectivity analysis, a large number of SEM images were acquired of the DSA patterns etched into 13 nm SiN, and defects were detected and classified according to the description provided in the methodology section. As shown in Figure 9, the majority of defects found in the DSA rectified patterns are partially closed holes. Missing holes and patches of missing holes are only rarely observed. Secondly, it can be observed that the defectivity is dropping rapidly as the guide pattern CD is increasing. For the best conditions evaluated here, the defect density was lower than 1 defect per 10.000.000 inspected holes.

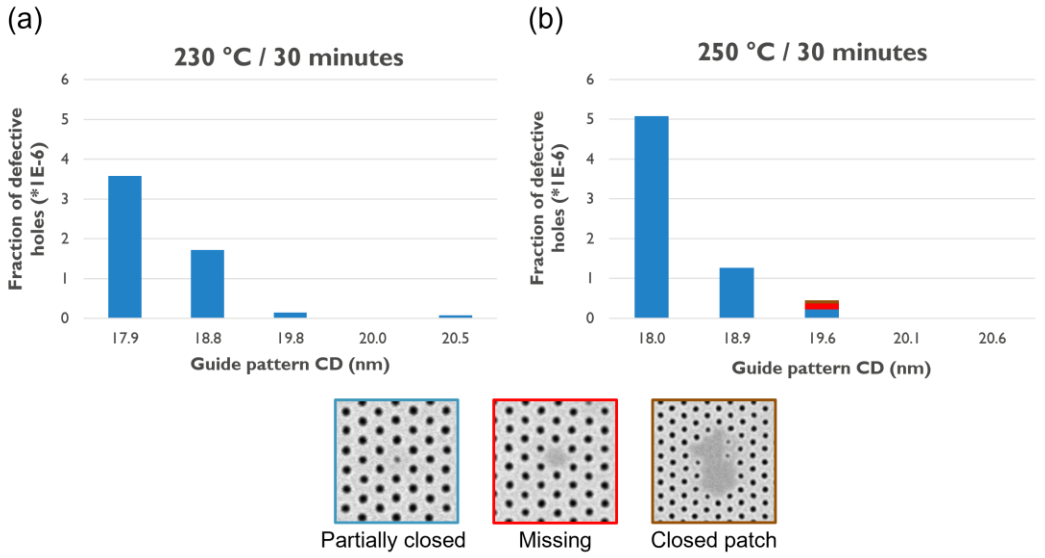


Figure 9. Defectivity analysis of a DSA rectified pitch$_{C2C}$ 36 nm EUV resist pattern as a function of guide pattern CD for two different thermal annealing conditions. Three types of defects were observed: partially closed holes (blue), missing holes (red), and patches of closed holes (brown). The data was acquired after pattern transfer of the DSA patterns into 13 nm SiN. 57.000.000 holes were inspected for each annealing condition (corresponding inspection area = 68.000 µm$^2$).

### 3.4 Pitch 34 nm HEXCH patterning

Finally, the possibility to reduce the EUV exposure dose followed by DSA rectification was explored. Three EUV resist materials having different EUV sensitivity were studied here. As shown in Figure 10, the LCDU of the resist pattern goes up as the sensitivity for EUV photons increases (printing at lower dose). This trade-off between EUV dose and pattern uniformity is well-known and represents a fundamental challenge for EUV lithography. As shown in Figure 10, DSA can avoid this trade-off by rectifying the EUV resist patterns. The LCDU after DSA rectification remains constant through dose even when using the most sensitive EUV resist material. Furthermore, defects from the low dose EUV resist pattern are rectified as well. As such, a dose reduction of about 60% could be achieved without compromising LCDU or defectivity.

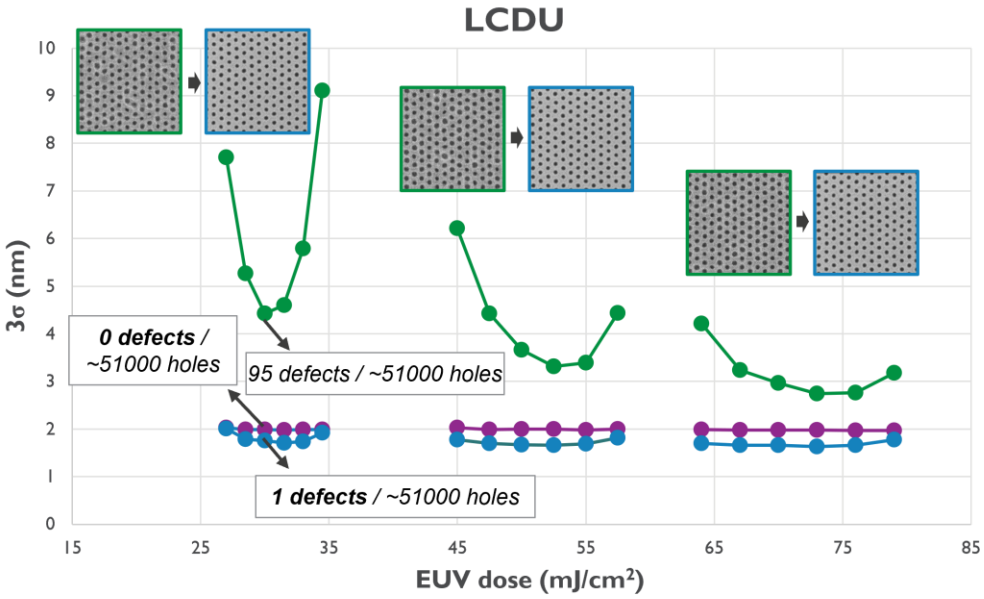


Figure 10. EUV dose reduction by DSA pattern rectification. Three EUV resists are evaluated having different EUV sensitivity. The LCDU values are given for the EUV resist pattern (green), DSA pattern after wet development (purple), and the DSA pattern after etch into 13 nm SiN (blue). Representative images of the EUV resist pattern and etched DSA pattern are inserted. Pitch of the pattern is 34 nm contact-to-contact.

## 4. CONCLUSIONS

In conclusion, the status of imec's DSA rectification process for both L/S and HEXCH EUV resist patterns has been evaluated. For rectified L/S patterns, bridge defects were found to be the most dominant defect type especially at pitch 24 nm. Tuning the BCP material formulation was shown to be an effective knob for reducing the bridge defect density, although other strategies are currently also under investigation. In case of HEXCH patterns, findings ways to control the PPE of the DSA patterns is identified as the major challenge for improving the rectification process. While some advances were made in this study, more efforts will be needed. In this context, the use of high-chi BCP materials might be of interest. Finally, a 60% EUV dose reduction was demonstrated for creating a $pitch_{C2C}$ 34 nm HEXCH pattern without compromising the LCDU or defectivity.

## ACKNOWLEDGEMENTS

The authors are grateful to the material suppliers for providing X-PS and BCP materials in the framework of joint development projects. The authors also kindly acknowledge the support for BCP processing by the track tool supplier in

the framework of a joint development project. The technical support of imec colleagues Nadia Vandenbroeck and Waut Drent is also kindly acknowledged.

## REFERENCES

[1] Biafore, J. J., Smith, M. D., Mack, C., Thackeray, J. W., Gronheid, R., Robertson, S. A., Graves, T. and Blankenship, D., "Statistical simulation of resist at EUV and ArF", Proc. SPIE 7273, 727343 (2009).
[2] De Silva, A., Meli, L., Goldfarb, D. L. and Felix, M., "Fundamentals of resist stochastics effect for single-expose EUV patterning", Proc. SPIE 10957, 109570F (2019).
[3] Neisser, M., "International roadmap for devices and systems lithography roadmap", J. Micro/Nanopattern. Mater. Metrol. 20(4), 044601 (2021).
[4] Delgadillo, P. A. R., Thode, C. J., Nealey, P. F., Gronheid, R., Wu, H., Cao, Y., Neisser, M., Somervell, M. H. and Nafus, K., "Implementation of a chemo-epitaxy flow for directed self-assembly on 300-mm wafer processing equipment," J. Micro/Nanolith. MEMS MOEMS 11(3), 031302 (2012).
[5] Singh, A., Nam, J., Lee, J., Chan, T. C., Wu, H., Yin, J., Cao, Y., Gronheid, R., "Manufacturability of dense hole arrays with directed self-assembly using CHIPS flow," Proc. SPIE 9777, 97770P (2016).
[6] Stoykovich, M. P., Daoulas, K. C. Muller, M., Kang, H., de Pablo, J. J., Nealey, P. F., "Remediation of line edge roughness in chemical nanopatterns by the directed self-assembly of overlying block copolymer films," Macromolecules 43, 2334-2342 (2010).
[7] Ruiz, R., Kang, H., Detcheverry, F. A., Dobisz, E., Kercher, D.S., Albrecht, T. R., de Pablo, J. J. and Nealey, P. F., "Density multiplication and improved lithography by directed block copolymer assembly," Science 321 (5891), 936-939 (2008).
[8] Lai, H., Huang, G., Tian, X., Liu, Y. and Ji, S., "Engineering the domain roughness of block copolymer in directed self-assembly," Polymer 249, 124853 (2022).
[9] Van Bel, J., Verstraete, L., Suh, H. S., De Gendt, S., Bezard, P., Vallat, R., Vandereyken, J., Li, W., Beggiato, M., Tamaddon, A. H., Beral, C., Santos, A., Alperson, B., Her, Y., "EUV lithography line-space pattern rectification using block copolymer directed self-assembly: a roughness and defectivity study," submitted for publication in Proc. SPIE (2023).
[10] Edwards, E. W., Montague, M. F., Solak, H. H., Hawker, C. J. and Nealey, P. F., "Precise control over molecular dimensions of block-copolymer domains using the interfacial energy of chemically nanopatterned substrates," Adv. Mater. 16(15), 1315-1319 (2004).
[11] Chevalier, X., Nicolet, C., Gharbi, A., Pimenta-Barros, P., Tiron, R., Fleury, G., Hadziioannou, G., Iliopoulos, I., Navarro, C., "Blending approaches to enhance the structural order in block-copolymer's self-assemblies," Proc. SPIE 9425, 94251N (2015).